JACS Au
AN OPEN ACCESS JOURNAL OF THE AMERICAN CHEMICAL SOCIETY

pubs.acs.org/jacsau
Article

How *Axial* Coordination Regulates the Electronic Structure and C−H Amination Reactivity of Fe−Porphyrin−Nitrene?

Mayank Mahajan and Bhaskar Mondal*

Cite This: *JACS Au* 2023, 3, 3494−3505
Read Online

ACCESS | Metrics & More | Article Recommendations | Supporting Information

ABSTRACT: Detailed electronic structure and its correlation with the intramolecular C−H amination reactivity of Fe−porphyrin−nitrene intermediates bearing different "axial" coordination have been investigated using multiconfigurational complete active space self-consistent field (CASSCF), N-electron valence perturbation theory (NEVPT2), and hybrid density functional theory (DFT-B3LYP) calculations. Three types of "axial" coordination, −OMe/−O(H)Me (**1-Sul**/**2-Sul**), −SMe/−S(H)Me (**3-Sul**/**4-Sul**), and −NMeIm (MeIm = 3-methyl-imidazole) (**5-Sul**) mimicking serine, cysteine, and histidine, respectively, along with no axial coordination (**6-Sul**) have been considered to decipher how the "axial" coordination of different strengths regulates the electronic integrity of the Fe−N core and nitrene-transfer reactivity of Fe−porphyrin−nitrene intermediates. CASSCF-based natural orbitals reveal two distinct classes of electronic structures: Fe-nitrenes (**1-Sul** and **3-Sul**) with relatively stronger axial coordination (−OMe and −SMe) display "imidyl" nature and those (**2-Sul, 4-Sul,** and **6-Sul**) with weaker axial coordination (−O(H)Me, −S(H)Me and no axial coordination) exhibit "imido-like" character. A borderline between the two classes is also observed with NMeIm axial coordination (**5-Sul**). Axial coordination of different strengths not only regulates the electronic structure but also modulates the Fe-3d orbital energies, as revealed through the *d*−*d* transition energies obtained by CASSCF/NEVPT2 calculations. The relatively lower energy of Fe-3d_{z2} orbital allows easy access to low-lying high-spin quintet states in the cases of weaker "axial" coordination (**2-Sul, 4-Sul,** and **6-Sul**), and the associated hydrogen atom transfer (HAT) reactivity appears to involve two-state triplet-quintet reactivity through minimum energy crossing point (^{3,5}MECP) between the spin states. In stark contrast, Fe-nitrenes with relatively stronger "axial" coordination (**1-Sul** and **3-Sul**) undergo triplet-only HAT reactivity. Overall, this in-depth electronic structure investigation and HAT reactivity evaluation reveal that the weaker axial coordination in Fe−porphyrin−nitrene complexes (**2-Sul, 4-Sul,** and **6-Sul**) can promote more efficient C−H oxidation through the quintet spin state.

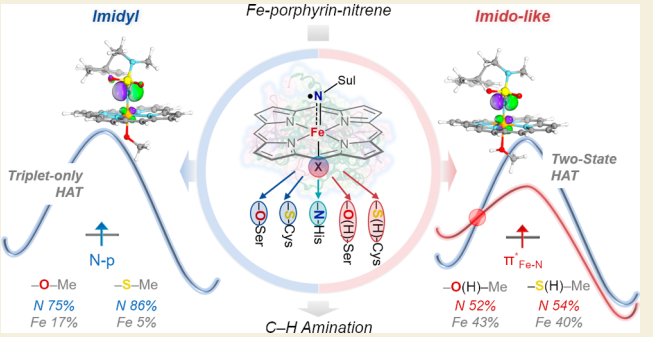

KEYWORDS: *Fe-porphyrin-nitrene, electronic structure, axial coordination, HAT, CASSCF/NEVPT2*

INTRODUCTION

Fe-porphyrin-nitrene species has been postulated to be the key intermediate in catalytic C−H amination reactions exhibited by heme-dependent enzymes[1−3] as well as synthetic metalloporphyrin catalysts.[4] The metal-bound nitrene moiety, Fe−NR (R = functional group attached to the nitrene), in these species, can efficiently and selectively transfer the redox-active nitrogen atom to C−H bonds leading to the formation of C−N bonds.[5−7] Such nitrene transfer commonly follows a single-electron transfer (SET) pathway due to the electronic nature of the Fe−N bond.[8,9] The Fe−nitrene bonding interactions in Fe-porphyrin-nitrenes can be described as analogous to Fischer-type nitrenes,[10] however, the bonding of the nitrene nitrogen with the partially filled Fe-d_π orbitals (Fe-d_{xz}/d_{yz}) may result in an unconventional electronic structure distinct from what one might expect for metal-nitrene species. Very recently, our group has established that the Fe-porphyrin-nitrene with *meso*-tetraphenylporphyrin (TPP) and NTos (Tos = tosyl) ligand architecture possesses an "imido-like" electronic character that can be best described as [(TPP)Fe^{IV}⋯NTos], which feature a Fe−N bond order of 1.5.[11] This electronic structure is an outcome of the bonding interaction between an intermediate spin (S = 1) Fe(IV) center with triplet nitrene (NR) leading to an overall triplet species, where one unpaired electron is based on Fe-$d_{xz/yz}$ and the other is based on the Fe−N antibonding π^* molecular orbital. Moreover, it was also shown that such an "imido-like" nature renders a relatively shorter M−N bond (1.71 Å) in Fe-porphyrin-nitrene as compared to a genuine "imidyl" M−N bond (1.80 Å) in Co-

Received: October 30, 2023
Revised: November 22, 2023
Accepted: November 27, 2023
Published: December 8, 2023

Scheme 1. Biocatalytic Nitrene-Transfer Reaction by Iron-Porphyrin Cofactor[a]

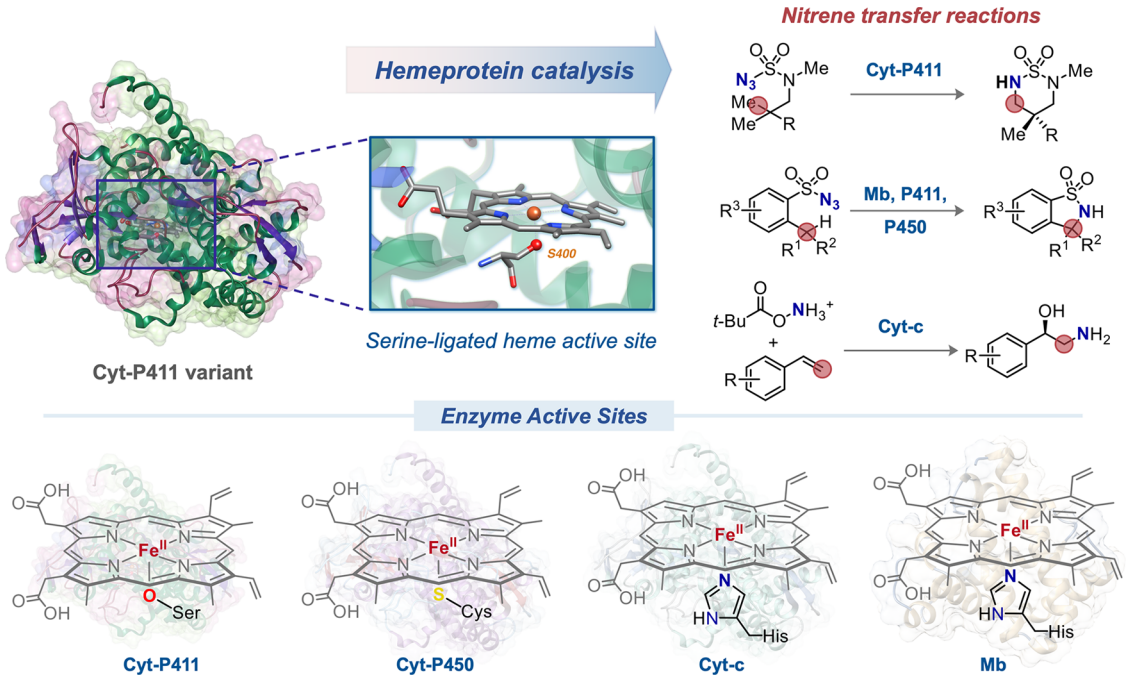

[a]Top panel: nitrene transfer reactions catalyzed by cytochrome- and myoglobin-based enzymes. Bottom panel: active sites of Cyt-P450, Cyt-P411, Cyt-c, and myoglobin (Mb) enzymes with "axial" O−Ser, S−Cys, and N−His coordination, respectively.

porphyrin-nitrene. Consequently, a relatively larger nitrene-transfer barrier ($\Delta G^{\ddagger}$ = 10.0 kcal/mol) was recorded for the Fe−porphyrin−nitrene as compared to that of the Co−porphyrin−nitrene ($\Delta G^{\ddagger}$ = 5.6 kcal/mol). This study exposed that the electronic integrity of the M−N interaction is extremely sensitive to the nature of the metal center, that is, the spin and oxidation state of the metal, which is closely dependent on the nature of the ligand environment, particularly the "axial" coordination.

The catalytic heart of heme-dependent enzymes commonly possesses a Fe(II)-porphyrin (heme) cofactor that differs in proximal "axial" amino acid coordination in the first coordination sphere of iron. Heme-containing enzymes, like cytochrome P450 (Cyt-P450), cytochrome c (Cyt-c), myoglobin (Mb), and their mutated forms possessing different "axial" coordination in the cofactor have been extensively explored for a versatile range of nitrene transfer reactions (Scheme 1). The first report of hemeprotein-catalyzed nitrene transfer reaction by Cyt-P450 dates back to 1985.[12] In 2014, Fasan and co-workers reported the intramolecular C−H amination of arylsulfonyl azides using Cyt-P450 enzymes possessing the cystine-ligated Fe-porphyrin cofactor.[13] The authors also reported the same intramolecular C−H amination using engineered and artificial myoglobin-based catalysts bearing a histidine-bound heme cofactor.[14] A similar C−H amination reactivity was also documented with an engineered serine-ligated Cyt-P450, known as Cyt-P411, by Arnold and co-workers.[15] Relatively recently, Arnold and co-workers reported enantioselective aminohydroxylation of styrenyl olefins by Cytochrome c bearing a Fe−porphyrin cofactor ligated with histidine.[16] These remarkable reports with wild-type and engineered enzymes not only demonstrate the versatility of the Fe-porphyrin platform toward catalytic nitrene transfer reactions but also indicate possible roles of the "axial" amino acid coordination in the overall reactivity. Pursuing this, Fasan and co-workers confirmed the effect of proximal coordination on nitrene transfer reactivity of myoglobin through substitution of the "axial" histidine coordination with natural residues, like Cys, Ser, Tyr, and Asp.[17] The observations on the effect of "axial" ligand present an intriguing question on how different coordination regulates the electronic structure of the catalytic resting state and, most importantly, of the metal-nitrene intermediate. In this context, Shaik and co-workers observed that "axial" serine coordination with Fe(II)−porphyrin complex results in a triplet ground state with σ^*_{Fe-O} mostly contributed by the Fe-d_{z2} orbital, whereas the same complex exhibits a quintet ground state on cysteine ligation and the Fe-cysteine antibonding interaction is dominated by the S-p orbital of cysteine.[18] In recent times, a computational investigation on the "axial" ligand effect was pursued by Zhang and co-workers, where the cysteine vs serine coordination was investigated through SH^-, MeO^-, and MeOH model coordination.[19] This work mainly reported the effect of the "axial" coordination on metal-nitrene formation and C−H amination reaction barriers. Considering the versatility in the "axial" coordination, that is, serine, cysteine, and histidine, in heme-dependent enzymes exhibiting nitrene transfer reactions and its role in reactivity, it would be of utmost importance to decipher how different "axial" coordination regulates the sensitive electronic structure of the Fe−Nitrene (Fe−NR) moiety,[11] and thereby, renders distinct reactivity.

In an attempt to uncover the influence of the "axial" coordination on the electronic structure integrity of the Fe-nitrene and its correlation with the nitrene transfer reactivity, we perform an in-depth electronic structure and C−H amination reactivity study based on multiconfigurational complete active space self-consistent field (CASSCF), N-electron valence perturbation theory up to second order corrections (NEVPT2), and hybrid density functional theory (DFT) calculations with six model Fe(II)−porphyrin com-

https://doi.org/10.1021/jacsau.3c00670
JACS Au 2023, 3, 3494−3505

Scheme 2. (a) Fe(II)-Porphyrin Model Complexes Mimicking the Axially Coordinated Heme Unit of Cytochrome P411 (1,2), Cytochrome P450 (3,4), Cytochrome c and Myoglobin (5), and No "Axial" Coordination (6); (b) Proposed Mechanism for Intramolecular C−H Amination of Sulfamoyl Azide (Sul) to Cyclic Sulfamide Catalyzed by Fe−Porphyrin Complexes

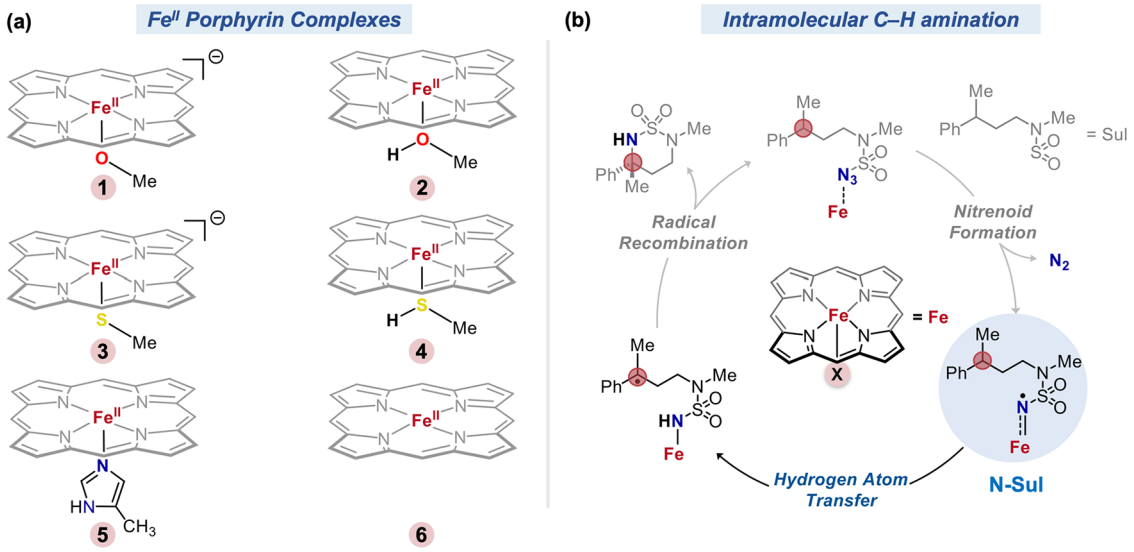

plexes (**1**−**6**). Complexes **1**−**6** were considered to mimic the axially coordinated heme unit of cytochrome P411 (**1**,**2**), cytochrome P450 (**3**,**4**), cytochrome c and myoglobin (**5**), and no "axial" coordination (**6**) (Scheme 2a). In these complexes, serine (Ser), cysteine (Cys), and histidine (His) coordinations have been modeled as −OMe, −SMe, and −NMeIm (MeIm = 3-methyl-imidazole), respectively. Both deprotonated (**1**,**3**) and protonated (**2**,**4**) forms of −OMe and −SMe coordination were considered, respectively. To probe the electronic structure of the Fe-porphyrin-nitrene species and its nitrene transfer reactivity, we selected the C(sp^3)−H amination reaction of sulfamoyl azide (**Sul**) to cyclic sulfamide reported by Arnold and co-workers (Scheme 2b).[20] This intramolecular C−H amination reaction follows three distinct reaction steps, namely, (i) generation of the metal-bound nitrene species ***N*-Sul** (*N* = 1−6, Sul = sulfamoyl), (ii) abstraction of hydrogen atoms (HAT) by the nitrene radical, and (iii) radical recombination to form the cyclic sulfamide. To establish the correlation between the electronic structure of Fe−porphyrin−nitrene and its nitrene transfer reactivity, we particularly focus on the second step, that is, the HAT exhibited by ***N*-Sul**. Overall, the current study primarily aims at uncovering the "true" electronic nature of the Fe−porphyrin−nitrene species in the presence of different "axial" coordination and its correlation with the nitrene-transfer chemistry.

COMPUTATIONAL METHODS

Calculations of equilibrium geometries, transition states, and harmonic vibrational frequencies were performed at the density functional theory (DFT) level by employing the Gaussian 16[21] suite of quantum chemical programs. Hybrid DFT B3LYP (Becke's three-parameter exchange and the Lee−Yang−Parr correlation)[22,23] functional was used for all the geometry optimizations and frequency calculations. It is noteworthy that the DFT-B3LYP functional has been widely used in the literature to study similar metal-nitrene and -carbene species,[9,11,18,20,24,25] which further supports its reliability for the electronic structure and reactivity of Fe-nitrene species calculated in this study. The geometry optimizations were performed using all-electron Ahlrichs double-ξ basis set def2-SVP[26] for H, C, N, O, and S atoms and the def2-TZVP[27] basis set for the central Fe atom. The effects due to dispersion were accounted for by using Grimme's D3 dispersion along with Becke−Johnson damping (D3BJ).[28] Single-point energy calculations were performed at the DFT-B3LYP level using the triple-ξ basis set def2-TZVP for all atoms. The effect due to solvation was accounted for through the implicit solvation model based on density (SMD)[29] involving chlorobenzene (ε = 5.7) as the solvent, which was also previously suggested by Shaik and co-workers[30] to mimic the enzymatic environment. To obtain the open-shell singlet (OSS) wave function, the converged triplet (S = 1) wave function was used as an initial guess, where the resulting wave function features a $<S^2>$ value of ∼0.9 that lies between $<S^2>$ of 0.0 and 2.0 for closed-shell singlet and triplet spin states, respectively. All the located transition states were confirmed to be first-order saddle points having only one imaginary frequency corresponding to the reaction coordinate. Intrinsic reaction coordinate (IRC) calculations were performed on transition state geometry to ensure connectivity of the TS to the proper reaction intermediates. Minimum energy crossing points (MECPs) were located using EasyMECP python script, which was written based on J. N. Harvey's Fortran code.[31,32]

Multiconfigurational complete active space self-consistent field (CASSCF)[33] calculations were performed on the DFT-B3LYP optimized geometries. CASSCF calculations were performed in conjunction with Ahlrichs triple-ξ basis set def2-TZVPP containing double polarization functions. The auxiliary basis set def2-TZVPP/C for correlation calculations against the orbital basis def2-TZVPP was used for the CASSCF calculations. A balanced active space was constructed with an appropriate combination of bonding and antibonding orbitals, involving the bonding (σ_{eq}) and antibonding (σ^*_{eq}) combination of porphyrin nitrogen and Fe-d_{x2-y2}, bonding (σ_{ax}) and antibonding (σ^*_{ax}) combinations of nitrene-nitrogen p_z and Fe-d_{z2}, π-bonding (π_y) and antibonding (π^*_y) combinations of nitrene-nitrogen p_y and Fe-d_{yz}, nonbonding

https://doi.org/10.1021/jacsau.3c00670
JACS Au 2023, 3, 3494−3505

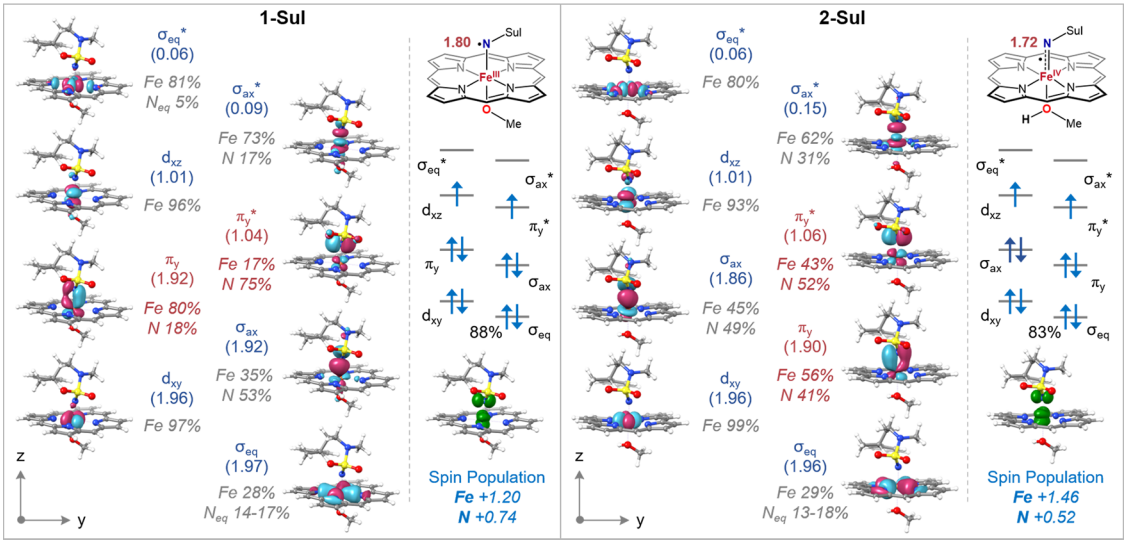

Figure 1. Electronic structure of Fe-porphyrin-nitrene derived from **1** (**1-Sul**, left) and **2** (**2-Sul**, right) showcasing natural orbitals, occupation numbers in parentheses, atomic orbital contributions, dominant electronic configuration, spin density, and spin population derived from the CASSCF(10,13)/def2-TZVPP level of theory. The orbitals are schematically arranged based on their occupation numbers, and the metal 4*d* orbitals are omitted for clarity. The chemical structures of **1-Sul** and **2-Sul** are presented with the Fe−N bond distance in Å.

Fe-d_{xy}, and Fe-d_{xz} orbitals. Five Fe-4d orbitals were added to the active space on top of the primary orbitals to account for the correlation effect due to the double d-shell. This resulted in an active space of 10 electrons distributed over 13 orbitals, CASSCF(10,13). Such balanced active spaces consisting of bonding, antibonding, nonbonding orbitals, and double d-shells have been reported to produce reliable electronic structures and spectroscopic parameters.[34,35] To account for the dynamical electron correlation effects, particularly to estimate the *d*−*d* transition energies, N-electron valence perturbation theory up to second order correction (NEVPT2)[36] calculations were performed using the CASSCF-(10,13) wave function. All of the multiconfigurational CASSCF and CASSCF/NEVPT2 calculations were performed using the ORCA 4.2.1 quantum chemical program.[37]

RESULTS AND DISCUSSION

Electronic Structure of Fe-Porphyrin-Nitrene Derived from Complexes 1 and 2

Before delving into the detailed electronic structure analysis of Fe-porphyrin-nitrene complexes, it is crucial to verify the accuracy of the geometry predicted by DFT methods, and, most importantly, the axial Fe−N(nitrene) bond. Geometry optimization of the Fe-porphyrin-nitrene species derived from complex **1** and **2**, that is, **1-Sul** and **2-Sul** at the OPBE (0% HF exchange) and B3LYP (20% HF exchange) levels yielded slightly different Fe−N bond distances (Table S1). Therefore, to make an unambiguous choice of the DFT method, we used a computational protocol involving the CASSCF(10,13)/NEVPT2 energy evaluation for a series of axial Fe−$N_{nitrene}$ (Fe−N) distances on the OPBE geometries of **1-Sul** and **2-Sul** (Figures S1 and S2). Specifically, a relaxed geometry scan of the Fe−N bond was performed using the OPBE functional followed by CASSCF(10,13)/NEVPT2 energy evaluation at each geometry on the potential energy surface. This way, we obtained the optimal Fe−N distance from the minimum energy structure predicted at the CASSCF(10,13)/NEVPT2 level. For complexes, **1-Sul** and **2-Sul**, the Fe−N distance predicted at the CASSCF(10,13)/NEVPT2 level appears closest to the B3LYP-optimized distance (Figures S1 and S2). A very similar result was also obtained for the complex lacking trans coordination **6-Sul** (Figure S3). These analyses unambiguously support the B3LYP functional to predict reliable electronic structure and geometry of the Fe−porphyrin−nitrene complexes investigated in the current work.

Fe−porphyrin−nitrene species are known to possess a triplet ground state,[9,11,18,20,38−42] which was also verified with the current complexes derived from **1**−**6** at the DFT-B3LYP level of theory (Table S1). In the following discussion, we will initially present the electronic structure investigation of the Fe−porphyrin−nitrene species **1-Sul** and **2-Sul** followed by a generalization for all of the complexes, **1-Sul** to **6-Sul**. For this purpose, multiconfigurational CASSCF(10,13) calculations were performed on the DFT-B3LYP optimized geometries of **1-Sul** and **2-Sul**. Consistent with the DFT results, the CASSCF(10,13)/NEVPT2 calculation also predicts a triplet ground state for **1-Sul** and **2-Sul** (Table S2).

As predicted by the CASSCF(10,13) calculation, the wave function for the triplet ground state of **1-Sul** is composed of a principal electronic configuration of $(\sigma_{eq})^2(d_{xy})^2(\sigma_{ax})^2(\pi_y)^2(\pi_y^*)^1(d_{xz})^1(\sigma_{ax}^*)^0(\sigma_{eq}^*)^0$ (88%), where the remaining configurations contribute <5% weightage to the ground state wave function (Figure 1, Table S3). The low-lying singlet of **1-Sul** appears to be of a significant multiconfigurational nature, as two major singlet configurations contribute to the wave function (Table S3). This is expected as a "pure" closed-shell singlet configuration is not possible for the Fe-porphyrin-nitrene consisting of unpaired electron densities centered on both Fe and nitrene nitrogen. In the ground triplet state of **1-Sul**, the natural orbitals derived from the CASSCF calculation clearly reveal two distinct bonding interactions between Fe and nitrene−nitrogen along the "axial" direction; a σ-bond formed between Fe-d_{z2} and N-p_z (σ_{ax}: 35% Fe + 53% N) and a rather weak π-interaction shaped between Fe-d_{yz} and N-p_y (π_y: 80% Fe + 18% N) featuring a prevailing Fe contribution. This leaves the antibonding π-orbital (π_y^*) mainly centered on N-p_y (75% N) with an occupation number

https://doi.org/10.1021/jacsau.3c00670
JACS Au 2023, 3, 3494−3505

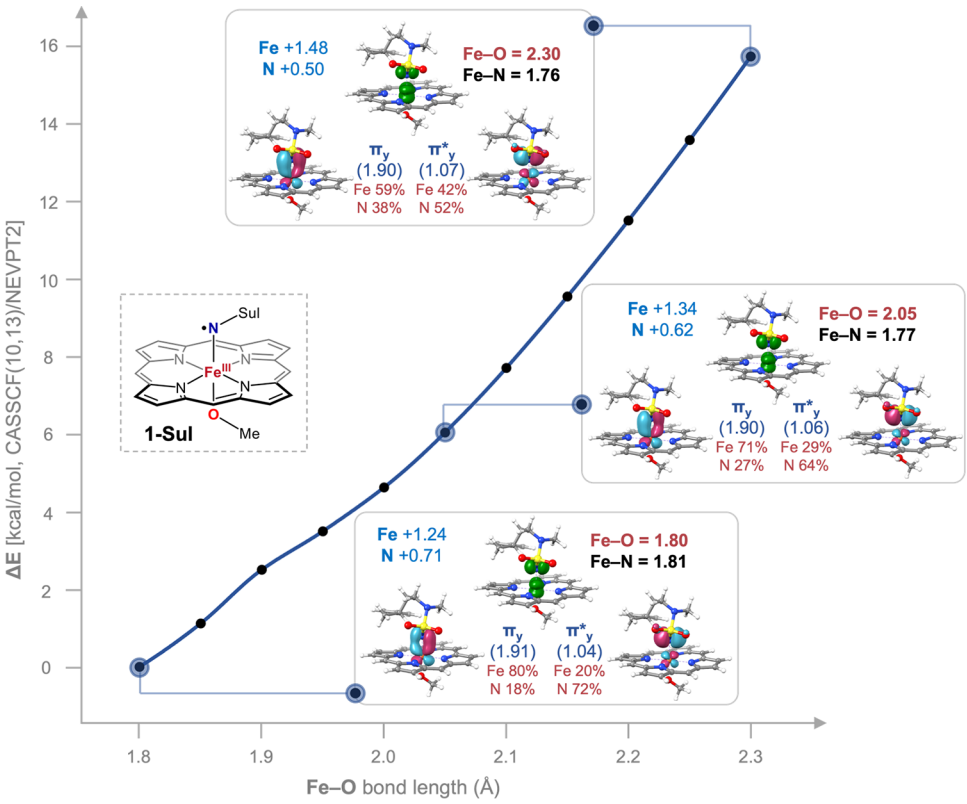

Figure 2. Evolution of the Fe−N π electronic structure with the "axial" Fe−O distance in **1-Sul** obtained at the CASSCF(10,13)/NEVPT2 level of theory.

(ON) of 1.04. On the other hand, the doubly occupied Fe-d_{xy} (ON = 1.96) and singly occupied Fe-d_{xz} (ON = 1.01) orbitals essentially remained nonbonding with Fe contributions of 97 and 96%, respectively. Apparently, the two singly occupied molecular orbitals (SOMOs) are predominantly based on the Fe-d_{xz} (d_{xz}) and N-p_y (π_y*) orbitals in **1-Sul**, which is also mirrored in the calculated spin-density resembling the combined shape of the SOMOs (Figure 1). The corresponding spin populations on Fe (+1.20) and N (+0.74), both close to 1.00, advocate for a low-spin (S = 1/2) Fe(III)-center ferromagnetically coupled with the N-centered radical ($^{\bullet}$N−Sul) in the triplet ground-state of **1-Sul**. Such an electronic structure scenario can be conclusively ascribed to a Fe(III)-imidyl (Fe^{III}−$^{\bullet}$*N*Sul) species, resembling the spectroscopically characterized genuine Co(III)-imidyl[43,44] species. The Fe(III)-imidyl nature of **1-Sul** renders a relatively elongated Fe−N bond (1.80 Å) with a formal bond order of 1.00. It is noteworthy to mention here that the calculated Fe−N bond distance in **1-Sul** is very similar to the Co−N distance (1.81Å) obtained for the well-characterized Co(III)-imidyl species [Co^{III}(TPP)($^{\bullet}$NNs)],[44] which further supports the "imidyl" nature of **1-Sul**.

In contrast to **1-Sul**, a dramatic difference in the electronic structure of the Fe−N π moiety was observed for **2-Sul** bearing a protonated and, therefore, much weaker −O(H)Me "axial" coordination. Specifically, the Fe−N π-interaction between Fe-d_{yz} and N-p_y (π_y) becomes rather covalent in nature featuring similar contributions from the two participating atoms, Fe 56% + N 41% (Figure 1). Consequently, a comparable atomic orbital contribution from Fe-d_{yz} and N-p_y (Fe 43% + N 52%) was also recorded in the antibonding π_y* orbital. This bonding scenario is in stark contrast to the **1-Sul**, where a rather ionic picture for the Fe−N π-interaction was observed (*vide supra*). As depicted in Figure 1, the stronger Fe−N π-interaction largely affected the spin population on Fe and N. Specifically, in **2-Sul**, the spin population on Fe (+1.46) is a 22% increase, and that on N (+0.52) is a 30% decrease as compared to what was observed in **1-Sul**. This scenario of the spin population on Fe and N significantly greater and lower than + 1.00, respectively, suggests an intermediate spin (S = 1) iron(IV) center interacting with the nitrene nitrogen resulting in an "imido-like" [Fe^{IV}⋯NSul] nature for **2-Sul**. We use the term "imido-like" to describe the electronic nature as a pure "imido" will have the entire spin population localized on the iron center bound to an N^{2-} moiety. The Fe(IV) imido-like nature was further corroborated by a rather shortened Fe−N bond distance of 1.72 Å, which is a ∼5% decrease compared to that of the **1-Sul** analogue. This is a clear consequence of the weakened "axial" coordination in **2-Sul** due to −O(H)Me (Fe−O = 2.16 Å) as compared to the **1-Sul** bearing −OMe (Fe−O = 1.86 Å).

Although the CASSCF(10,13) electronic structures are qualitatively well reproduced at the DFT-B3LYP level, a fundamental difference between the CASSCF and DFT levels appears at the degree of metal−ligand covalency. For instance, at the DFT level, a similar degree of covalency is estimated for Fe−N π-antibonding orbital (π_y*) for both **1-Sul** (Fe 41% + N 44%) and **2-Sul** (Fe 40% + N 48%) (Figures S4 and S5). This is somewhat counterintuitive, as the Fe−N bond in **1-Sul** (1.80 Å) is longer than that of the **2-Sul** (1.72 Å) (Figures 1 and S4, S5). The same Fe−N covalency, **1-Sul** (Fe 17% + N 75%) and **2-Sul** (Fe 43% + N 52%) are properly described at the CASSCF(10,13) level, which corroborates well with the calculated Fe−N bond distance (Figures 1 and S4,S5). This

https://doi.org/10.1021/jacsau.3c00670
JACS Au 2023, 3, 3494−3505

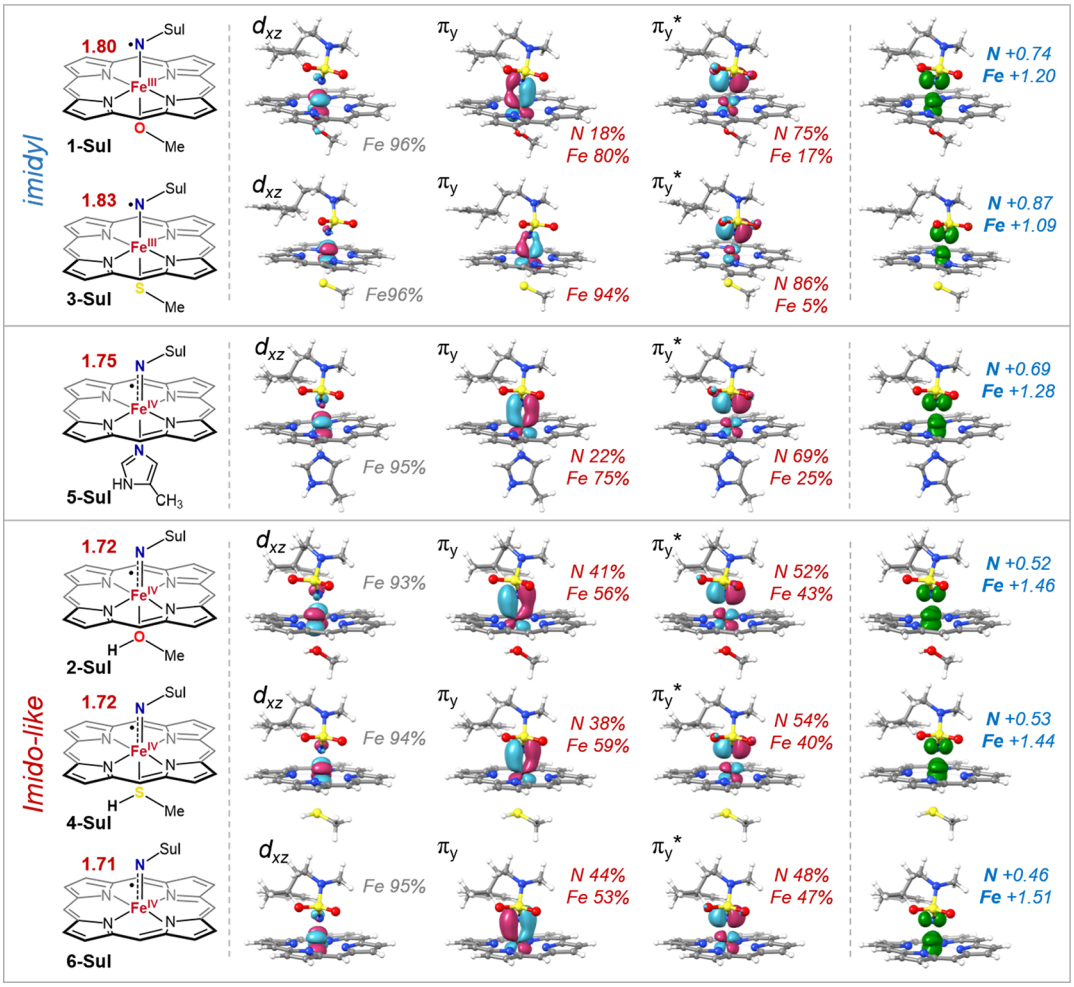

Figure 3. Key orbitals describing the Fe−N π-interaction in Fe-porphyrin-nitrene species derived from complexes **1**−**6** and sulfamoyl azide, **1-Sul**, **2-Sul**, **3-Sul**, **4-Sul**, **5-Sul**, and **6-Sul**. Left panel: chemical structure and Fe−N distance in Å. Middle panel: key π-natural orbitals along with the atomic contributions from Fe and N. Right panel: spin density and spin population obtained at the CASSCF(10,13) level of theory.

justifies the essentiality of the ab initio multiconfigurational CASSCF calculation to establish a proper electronic structure description of the Fe-porphyrin-nitrene complexes.[11]

Electronic Structure Evolution with "Axial" Coordination

The distinct electronic structures of **1-Sul** and **2-Sul** differing in the strength of "axial" coordination prompted us to inspect how the Fe−N π interactions evolve with the "axial" Fe−O distance. For this purpose, we generated several geometries on the potential energy surface through a relaxed scan of the "axial" Fe−O bond, followed by CASSCF(10,13)/NEVPT2 energy calculations at each point (Figure 2). As one proceeds from the near-equilibrium structure of **1-Sul** (Fe−O = 1.80 Å, Fe−N = 1.81 Å) to the point with an elongated Fe−O distance, appreciable changes in the Fe−N π interaction were observed. For instance, at the point with Fe−O = 2.05 Å, the Fe−N distance shrinks to 1.77 Å, and consequently, the Fe−N π-antibonding orbital (π_y*) gets a lesser N-p_y character and larger Fe-d_{yz} character, forwarding toward stronger covalency. This effect becomes more prominent at a Fe−O distance of 2.30 Å, where the Fe−N bond distance (1.76 Å) becomes similar to that of the **2-Sul**. At this point, a comparable Fe and N contribution, 42% and 52%, respectively, clearly reveals a covalent Fe−N π-bonding interaction, as was observed in **2-Sul**. Throughout the structural evolution of Fe−O coordination, the spin population on N decreases from +0.71 to +0.50 and that of Fe increases from +1.24 to +1.48, suggesting intermediate spin (S = 1) Fe(IV) character developed at a weakened Fe−O coordination (Figure 2). The same electronic structure evolution analysis was also performed with **2-Sul** by systematically shortening the Fe−O distance close to its equilibrium position of 2.30 to a shortened distance of 1.80 Å (Figure S10). These electronic structure evolution studies nicely rationalize the "imidyl" nature of **1-Sul** and the "imido-like" nature of **2-Sul** featuring stronger and weaker Fe−O coordination, respectively.

Electronic Structure in Different "Axial" Coordination Environments

Evidently, the strength of the "axial" coordination has a profound influence on the electronic integrity of the Fe−N π moiety, as established with **1-Sul** and **2-Sul** possessing "imidyl" and "imido-like" characters, respectively. This observation led us to pursue a parallel electronic structure comparison of the Fe−N π moiety for all six Fe-porphyrin-nitrene species derived from complexes **1**−**6** (Figure 3). **3-Sul**, bearing a −SMe "axial" coordination, displays a very similar electronic structure to that observed for **1-Sul** with a marginal increase and decrease in nitrogen and iron spin populations, respectively (Figures 3 and S6). In **3-Sul**, the Fe−N π_y* orbital is dominated by N-p_y

https://doi.org/10.1021/jacsau.3c00670
JACS Au 2023, 3, 3494−3505

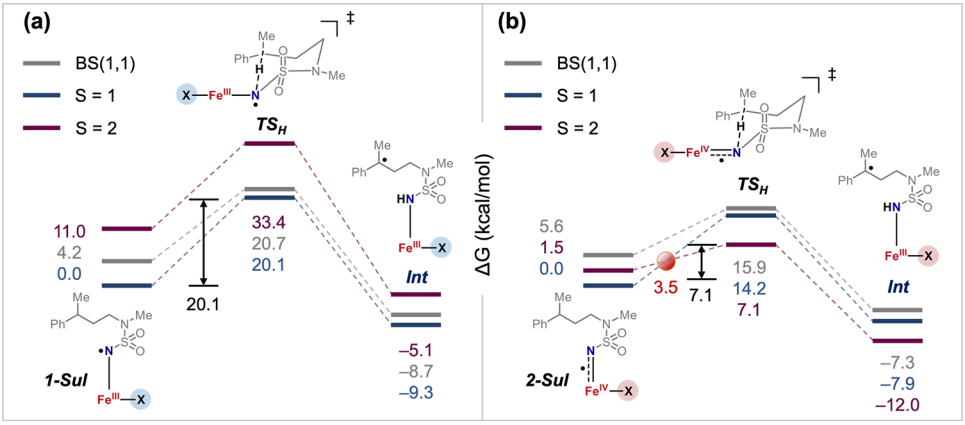

Figure 4. Reaction free energy (ΔG) profile for the hydrogen atom transfer (HAT) reaction exhibited by **1-Sul** (a) and **2-Sul** (b) in three different spin states. Results were obtained at the DFT-B3LYP/def2-TZVP/SMD (chlorobenzene) level of theory.

character (86%), and the corresponding N spin population (+0.87) becomes close to 1.00, suggesting an "imidyl" nature for the Fe–N moiety. Akin to that of **1-Sul**, an elongated Fe–N bond distance of 1.83 Å further corroborates the Fe(III)–$^{\bullet}$NSul imidyl nature for **3-Sul**. Such an elongated Fe–N bond, and therefore, the "imidyl" nature of **1-Sul** and **3-Sul**, can be attributed to their strong anionic "axial" coordination through –OMe and –SMe. On the other hand, the protonated form of the –SMe coordination, i.e., –S(H)Me in complex **4-Sul** exerts a similar electronic structure modulation as observed in the case of its methoxy (**2-Sul**) analogue. The Fe–N π_y* becomes covalent in nature in **4-Sul** with 40% Fe and 54% N character, and consequently, a rather short Fe–N distance of 1.72 Å was recorded (Figures 3 and S7). Like **2-Sul**, the increased and decreased spin population on Fe (+1.44) and N (+0.53), respectively suggests an "imido-like" nature for **4-Sul**.

The Fe-porphyrin-nitrene species **6-Sul** lacking any "axial" coordination exhibit an electronic structure analogous to that of **2-Sul** and **4-Sul**, where the Fe–N π interaction is of pure covalent nature with almost equal contribution from the Fe-d_{yz} and N-p_y (Figures 3 and S9). The covalent nature of the Fe–N π interaction is evident from the CASSCF(10,13)-derived natural orbitals of **6-Sul**, π_y (Fe 53% + N 44%), and π_y* (Fe 47% + N 48%). This electronic structure scenario is similar to what was obtained for **2-Sul** and **4-Sul** bearing –O(H)Me and –S(H)Me "axial" coordination, respectively. This, indeed, indicates the –O(H)Me and –S(H)Me coordination to be a very weak one. This is also reflected in the matching Fe–N bond lengths of 1.72, 1.72, and 1.71 Å in **2-Sul**, **4-Sul**, and **6-Sul**, respectively (Figure 3). In line with this, the spin populations on Fe +1.51 and N +0.46 in **6-Sul** are also analogous to those obtained with **2-Sul** and **4-Sul**. Therefore, a highly covalent Fe–N π interaction along with Fe and N spin population significantly away from 1.00 suggests an iron(IV)-imido-like nature (Fe^{IV}···NSul) for **6-Sul**. Apparently, the weak (in **2-Sul** and **4-Sul**) or no (in **6-Sul**) "axial" coordination renders a much stronger Fe–N interaction with enhanced π-bonding, leading to an "imido-like" electronic nature.

The species **5-Sul** bearing –N(imidazole) "axial" coordination exhibits an electronic characteristic somewhat between "imidyl" and "imido-like" (Figures 3 and S8). Specifically, the Fe and N contributions to the bonding π_y (Fe 75% + N 22%) and antibonding π_y* (Fe 25% + N 69%) orbitals get noticeably altered as compared to the **1-Sul** and **2-Sul**, and an appreciable shortening of the Fe–N bond to 1.75 Å and change in spin population on Fe (+1.28) and N (+0.69) were observed in **5-Sul**. Because of the moderate coordination strength of –N(imidazole), which may be considered intermediate between –OMe/–SMe and –O(H)Me/–S(H)Me, the electronic nature of the Fe–N core in **5-Sul** somewhat appears at a borderline between Fe(III)-imidyl and Fe(IV)-imido-like, as evident from the atomic orbital contribution. The spin population on N (+0.69) and Fe (+1.28) in **5-Sul** also corroborated well with the intermediacy of the between "imidyl" and "imido-like" electronic nature.

Nitrene-Transfer Reactivity

As perceived through the CASSCF-based electronic structure analysis, the Fe–N π-character and spin population on the N-atom of Fe-porphyrin-nitrene species dramatically vary under the influence of the "axial" coordination. This would apparently affect the nitrene transfer step, that is, the hydrogen atom transfer (HAT) leading to the C–H amination (Scheme 2b). To investigate how the electronic structure of the Fe–N π moiety can regulate the free energy barrier of the HAT step, we first computed the reaction energetics of this step for **1-Sul** and **2-Sul** at three spin states, open-shell singlet BS(1,1) (BS = broken symmetry), triplet, and quintet. **1-Sul** possessing a Fe(III)-imidyl Fe–N core exhibits the lowest free energy HAT pathway on the triplet (S = 1) surface with a barrier of 20.1 kcal/mol (**TS$_H$**, Figure 4a). The lowest energy triplet HAT pathway for **1-Sul** appears consistent with the literature reports for similar reactions mediated by Fe-porphyrin-nitrenes bearing a –OMe axial coordination.[9,20,38] The lowest energy triplet transition state is verified through intrinsic reaction coordinate (IRC) evaluation (Figure S11). In the transition state, one of the Fe-$d_{xz/yz}$ π-orbitals gets involved in the electron transfer process, suggesting a TS of π-nature (Figure S12). The free energy barriers associated with the BS(1,1) singlet and quintet (S = 2) states 20.7 and 33.4 kcal/mol, respectively (Figure 4a) are higher compared to the triplet state. The overall HAT process appears to be exergonic on all three spin surfaces.

In stark contrast to **1-Sul**, **2-Sul** featuring a Fe(IV)-imido-like Fe–N core displays the lowest free energy pathway on the quintet (S = 2) surface with a dramatically lower barrier of 7.1 kcal/mol (**TS$_H$**, Figures 4b, S11). The quintet TS is also of π-nature, where a spin-coupled orbital was observed between Fe-d_{yz} and a C-centered substrate radical (Figure S12).

https://doi.org/10.1021/jacsau.3c00670
JACS Au 2023, 3, 3494–3505

Interestingly, owing to a marginal triplet-quintet free energy separation (ΔG_{Q-T} = 1.5 kcal), the triplet ground state of **2-Sul** undergoes spin crossover to the quintet surface through a minimum energy crossing point (^{3,5}MECP) and exhibits exergonic HAT reactivity on the same surface. The MECP occurs around 3.5 kcal/mol above the triplet reactant complex on the free energy surface. The lengthening of the Fe−N bond to 2.048 Å clearly indicates that the MECP originates from the changes in the electronic structure of the iron-nitrene moiety (Figure S13). In addition, a distance scan along the Fe−N bond naturally yields a crossing point between the triplet and quintet spin surface (Figure S20). Notably, similar two-state HAT reactivity with a lower energy quintet transition state has also been reported in the literature for nonheme Fe(IV)-imido complexes,[45−47] suggesting an underlying "imido-like" electronic structure as established for **2-Sul**. The other two transition states, triplet and open-shell singlet, appear at higher free energies, 14.2 and 15.9 kcal/mol, respectively.

This dramatic difference in the HAT barrier between **1-Sul** and **2-Sul** is a clear consequence of their different electronic structures of the Fe−N core. The significantly lower free energy barrier for **2-Sul** ($\Delta G^{\ddagger}$ = 7.1 kcal/mol) as compared to **1-Sul** ($\Delta G^{\ddagger}$ = 20.1 kcal/mol) can be rationalized using the concept of exchange-enhanced reactivity (EER) coined by Shaik and co-workers, which states "pathways that increase the number of unpaired and spin-identical electrons on a metal center will be favored by exchange stabilization".[48] As **2-Sul** could easily access the high-spin quintet state (S = 2) through triplet-quintet spin crossover, the relatively lower HAT barrier is likely a result of the EER originating due to the large number of unpaired electrons on the high-spin surface. This observation falls in line with the terminal Fe(IV)-oxo chemistry, where electronic structure studies predicted that Fe^{IV}=O species in quintet spin state are better oxidants for HAT.[49−53] Therefore, based on the current electronic structure−reactivity correlation, one can qualitatively predict that Fe-porphyrin-nitrene complexes that undergo HAT reactivity via the quintet state will be a better oxidant. However, it should be noted that apart from the triplet-quintet two-state reactivity, the potency of the Fe−NR core to perform the HAT must be correlated with the N−H bond that forms as a result of the reaction.

Extending the investigation of the trans "axial" coordination effect on the HAT reactivity, a side-by-side comparison of the HAT barrier was made between **1-Sul**, **2-Sul**, **3-Sul**, **4-Sul**, and **6-Sul** on their triplet and quintet free energy surfaces (Figure 5). Fe-porphyrin-nitrene intermediate **3-Sul** possessing a trans "axial" −SMe ligand exhibits a HAT reactivity very similar to that observed for **1-Sul**. **3-Sul** has a well-separated triplet ground state (ΔG_{Q-T} = 9.3 kcal/mol) and undergoes a HAT reaction on the triplet surface with a free energy barrier of 18.4 kcal/mol, where the quintet HAT transition state lies at a high free energy of 30.0 kcal/mol. This observation of similar reactivity between **1-Sul** and **3-Sul** corroborates well with their similar electronic structure featuring a Fe(III)-imidyl Fe−N core. The protonated axial −S(H)Me coordinated analogue of **3-Sul**, i.e., **4-Sul** featuring Fe(IV)-imido-like Fe−N core undergoes a spin crossover from triplet to quintet surface owing to the low triplet-quintet separation (ΔG_{Q-T} = 4.0 kcal/mol, Figure 5). The accessibility of the quintet state results in a significantly lower HAT barrier of 9.2 kcal/mol, as compared to that of the **3-Sul**. The associated triplet transition state lies much higher in energy (17.2 kcal/mol) than the quintet one.

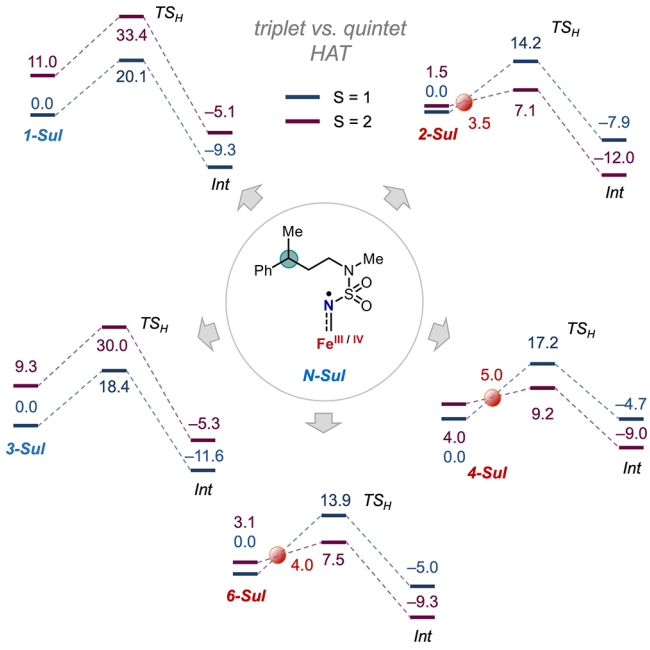

Figure 5. Triplet vs quintet hydrogen atom transfer (HAT) free energy profiles for **1-Sul**, **2-Sul**, **3-Sul**, **4-Sul**, and **6-Sul**. The red circles represent the calculated minimum energy crossing point (MECP) position between triplet and quintet spin states. Results were obtained at the DFT-B3LYP/def2-TZVP/SMD (chlorobenzene) level of theory.

Similar to the "imido-like" complex **2-Sul**, the spin crossover in **4-Sul** becomes apparent when the Fe−N scan on the triplet and quintet surface are plotted together (Figure S20) and an elongation of the Fe−N bond to 1.806 Å was observed in the MECP (Figure S18). Therefore, the imidyl/imido-like Fe−N cores in **1-Sul**/**2-Sul** and **3-Sul**/**4-Sul** pairs result in distinct HAT reactivity, with the "imido-like" core favoring two-state reactivity through a low-lying quintet pathway.

To further verify the weak axial ligand field effect on the reactivity, Fe-porphyrin-nitrene complex **6-Sul** lacking a trans "axial" coordination was subjected to the HAT reaction. Complex **6-Sul** undergoes HAT reactivity analogous to that observed with **2-Sul** and **4-Sul**. **6-Sul** also possesses a low triplet-quintet energy separation (ΔG_{Q-T} = 3.1 kcal/mol), which allows it to undergo spin crossover to the quintet surface through an MECP lying 4.0 kcal/mol above the triplet ground state. Like **2-Sul** and **4-Sul** a scan along the Fe−N bond on the triplet and quintet surface gives a crossing point between the triplet and quintet spin surface (Figure S20) and an elongation of the Fe−N bond to 1.781 Å was observed in the MECP (Figure S19). The minimum free energy triplet HAT barrier was calculated to be 7.5 kcal/mol, which is ∼6 kcal/mol lower as compared to the corresponding quintet surface. Thus, **2-Sul**, **4-Sul**, and **6-Sul** bearing weak or no trans "axial" coordination environment exhibit analogous HAT reactivity on the quintet surface, which can be attributed to their Fe(IV)-imido-like Fe−N core. In line with this, **5-Sul** possessing −N(imidazole) "axial" coordination also exhibits a spin crossover between the triplet and quintet (ΔG_{Q-T} = 6.4 kcal/mol) at 8.1 kcal/mol with reference to the triplet ground state (Figure S21). However, the quintet free energy barrier of 12.3 kcal/mol for the HAT appears close to the triplet one (13.7 kcal/mol). This also reflects the ambiguous electronic nature of the Fe−N moiety of **5-Sul** as discussed above. The detailed electronic

https://doi.org/10.1021/jacsau.3c00670
JACS Au 2023, 3, 3494−3505

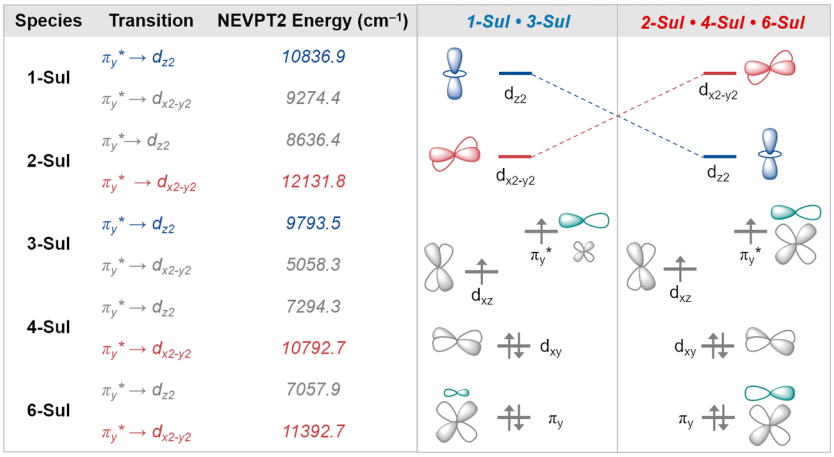

Figure 6. $d-d$ transition energies obtained at the CASSCF(10,13)/NEVPT2 level of theory and schematic orbital-splitting diagram for species **1-Sul**, **2-Sul**, **3-Sul**, **4-Sul**, and **6-Sul**.

structure of all the lowest energy transition states and their IRC profiles for the complexes **1-Sul** to **6-Sul** are presented in the Supporting Information (Figures S11,S12,S14−S17).

Effect of "Axial" Coordination on Orbital Energies

Evidently, the easy accessibility of the quintet state for the weak or no "axial" coordination is the origin of the distinct HAT reactivity calculated for **2-Sul**, **4-Sul**, and **6-Sul** as compared to **1-Sul** and **3-Sul**. It would be, therefore, intriguing to investigate how the "axial" coordination of different strengths governs the orbital energies, and thereby, the accessibility of the quintet state. Looking at the electronic distribution of the d-manifold of ***N*-Sul** species (Figure 1), the quintet spin state would be generated through a spin-flip electronic transition from the nonbonding Fe-d_{xy} orbital to either Fe-d_{z2}-based σ_{ax}* or Fe-d_{x2-y2}-based σ_{eq}* orbital. As such, the accessibility of the quintet state would depend on the relative energies of the Fe-d_{z2} and Fe-d_{x2-y2} orbitals. It should be noted that populating the Fe-d_{x2-y2} orbital in the quintet state would not affect the electronic structure and geometry of the Fe−N core, whereas populating the Fe-d_{z2} orbital would. To investigate the relative energies of the electron accepting orbitals (EAOs), Fe-d_{x2-y2} and Fe-d_{z2} to be occupied in the quintet state, we calculated the $d-d$ transition energies in the d-manifold using the NEVPT2 method on top of the CASSCF(10,13) wave function. This way, both static and dynamic electron correlation effects could be accounted for accurately estimating the transition energies. The main focus was on the $d-d$ transition energies for transitions $\pi_y^* \rightarrow d_{z2}$ and $\pi_y^* \rightarrow d_{x2-y2}$ in the ***N*-Sul** species (Figure 6), where the calculated transition energies should provide a good estimation of the relative energies of the two EAOs.

For Fe-nitrene species **1-Sul** and **3-Sul**, the $\pi_y^* \rightarrow d_{z2}$ transition appears at 10,836 and 9793 cm^{-1}, respectively, whereas the $\pi_y^* \rightarrow d_{x2-y2}$ transition appears at lower energies for both cases (Figure 6). This clearly suggests that the EAO Fe-d_{x2-y2} lies lower in energy as compared to Fe-d_{z2} and therefore would be populated in the quintet state of **1-Sul** and **3-Sul**. On the other hand, for species **2-Sul**, **4-Sul**, and **6-Sul**, the $\pi_y^* \rightarrow d_{z2}$ transition appears at 8636, 7294, and 7057 cm^{-1}, respectively, which is much lower in energy as compared to the $\pi_y^* \rightarrow d_{x2-y2}$ transition, 12131, 10792, and 11392 cm^{-1}, respectively. This clearly indicates the low-lying Fe-d_{z2} orbital as compared to Fe-d_{x2-y2} in **2-Sul**, **4-Sul**, and **6-Sul**. Effectively, the energy ordering of the EAOs, Fe-d_{x2-y2}, and Fe-d_{z2} can be considered swapped in species **2-Sul**/**4-Sul**/**6-Sul** as compared to that in **1-Sul**/**3-Sul** (Figure 6). This analysis of the $d-d$ transition energies nicely rationalizes the accessibility of the quintet state in the case of **2-Sul**, **4-Sul**, and **6-Sul** through an MECP involving the elongation of the Fe−N bond featuring the Fe-d_{z2}-based bonding and antibonding orbitals (σ_{ax} and σ^*_{ax}). On the other side, the Fe-d_{z2} orbital centered on the Fe−N core would not be populated in the quintet state of **1-Sul** and **3-Sul**, thereby rationalizing its triplet-only HAT reactivity. This observation concludes that a relatively stronger trans "axial" coordination (e.g., −OMe and −SMe in **1-Sul** and **3-Sul**) exerts much stronger interaction with the Fe-center which pushed the Fe-d_{z2} higher in energy relative to the Fe-d_{x2-y2}. A completely opposite scenario was observed in the case of a weaker (−O(H)Me, −S(H)Me) or no trans "axial" coordination environment, that is, in the case of **2-Sul**, **4-Sul**, and **6-Sul**. This is noteworthy to mention that both the $d-d$ transitions, $\pi_y^* \rightarrow d_{z2}$ and $\pi_y^* \rightarrow d_{x2-y2}$ appear at a similar energy range of ∼10500 cm^{-1} with the $\pi_y^* \rightarrow d_{z2}$ marginally higher in energy by ∼200 cm^{-1} in **5-Sul** (Table S4), which again corroborates with its mixed electronic nature.

CONCLUDING REMARKS AND OUTLOOK

The correlation between the electronic structure and C−H amination reactivity of Fe-porphyrin-nitrene intermediates bearing "axial" coordination of different strengths has been investigated in unprecedented detail using CASSCF, CASSCF/NEVPT2, and DFT calculations. The analyses could decipher how the "axial" coordination governs the true electronic nature of the Fe-porphyrin-nitrene species and their nitrene-transfer reactivity. Specifically, the CASSCF(10,13)-derived molecular orbitals along with the distribution of the spin-population on the Fe−N moiety reveal an "imidyl" (Fe^{III}−$^{\bullet}$NSul) nature for the Fe-nitrene intermediates bearing relatively stronger "axial" coordination, such as in **1-Sul** (−OMe) and **3-Sul** (−SMe). The same analysis uncovered an "imido-like" (Fe^{IV}⋯NSul) character for **2-Sul** (−O(H)Me), **4-Sul** (−S(H)Me), and **6-Sul** (no axial ligand) possessing a relatively weaker "axial" coordination. Complementing these electronic characteristics, an elongated Fe−N bond of ∼1.80 Å was observed in the first case and a shortened one of ∼1.72 Å for the latter.

The two distinct classes of electronic structures regulated by the "axial" coordination in Fe-porphyrin-nitrene intermediates

https://doi.org/10.1021/jacsau.3c00670
JACS Au 2023, 3, 3494−3505

were found to be elegantly correlated with the HAT reactivity. For the Fe(III)-imidyl species, that is, **1-Sul** and **3-Sul** bearing a stronger "axial" coordination, a triplet-only HAT reactivity initiated from the ground state was observed. On the other hand, for the Fe(IV)-imido-like species **2-Sul, 4-Sul**, and **6-Sul**, the quintet state featuring occupation in the Fe-3d_{z2}-based orbital becomes easily accessible, which triggers spin crossover between triplet and quintet and HAT reactivity through the quintet spin state was observed via two-state reactivity. The **5-Sul** displaying a borderline electronic character between "imidyl" and "imido-like" also exhibits two-state reactivity with comparable triplet and quintet HAT transition states involving a ^{3,5}MECP lying higher in free energy as compared to **2-Sul, 4-Sul**, and **6-Sul**.

This work, for the first time, establishes how the "axial" coordination of different strengths can regulate the electronic structure of the Fe−N moiety in Fe−porphyrin−nitrene species and their crucial hydrogen atom transfer reactivity. Based on the current findings, one can anticipate that the axial ligand can affect the potency of the Fe-porphyrin-nitrene toward HAT reactivity. The quantification of the HAT efficiency toward a range of substrates having different C−H bond dissociation free energies (BDFE) requires further computational investigations on a series of Fe-porphyrin-nitrene with varying trans coordination, which is ongoing in our laboratory. It should also be noted that the electronic structure and reactivity of the Fe−NR (R = functional group attached to the nitrene) core may be influenced by the type of the nitrene precursor, which is an open avenue for systematic experimental and computational studies. Overall, the current findings will contribute to a sound understanding of the true electronic structure of Fe-bound nitrenes in different "axial" coordination environments and can open new opportunities in designing novel synthetic catalysts for nitrene-transfer chemistry.

■ ASSOCIATED CONTENT

Supporting Information

The Supporting Information is available free of charge at https://pubs.acs.org/doi/10.1021/jacsau.3c00670.

Structure evaluation at different DFT methods; full electronic structures at the CASSCF level; electronic structure evolution studies; MECP geometries, HAT reactivity, and *d*−*d* transition energies; and optimized Cartesian coordinates for all the species involved (PDF)

■ AUTHOR INFORMATION

Corresponding Author

Bhaskar Mondal − *School of Chemical Sciences, Indian Institute of Technology Mandi, Mandi, Himachal Pradesh 175075, India;* orcid.org/0000-0001-9026-5974; Email: bhaskarmondal@iitmandi.ac.in

Author

Mayank Mahajan − *School of Chemical Sciences, Indian Institute of Technology Mandi, Mandi, Himachal Pradesh 175075, India*

Complete contact information is available at: https://pubs.acs.org/10.1021/jacsau.3c00670

Author Contributions

M.M. and B.M. designed the whole project. M.M. executed all the theoretical calculations. Both authors wrote the manuscript. CRediT: **Mayank Mahajan** conceptualization, data curation, formal analysis, investigation, methodology, writing-original draft; **Bhaskar Mondal** conceptualization, formal analysis, funding acquisition, investigation, supervision, writing-original draft, writing-review & editing.

Notes

The authors declare no competing financial interest.

■ ACKNOWLEDGMENTS

The authors are grateful for the funding support from the Science and Engineering Research Board (SERB) in the form of a Start-Up Research Grant (SRG/2020/000691) and a Seed Grant from IIT Mandi (IITM/SG/ABP/76). M.M. thanks the Ministry of Education (MoE) for the research fellowship. The High-Performance Computing (HPC) facility at IIT Mandi and PARAM Himalaya computing facility is acknowledged for providing high-end computational resources. The authors are further thankful to the reviewers for their constructive comments and suggestions.

■ REFERENCES

(1) Dunham, N. P.; Arnold, F. H. Nature's Machinery, Repurposed: Expanding the Repertoire of Iron-Dependent Oxygenases. *ACS Catal.* **2020**, *10*, 12239−12255.

(2) Yang, Y.; Arnold, F. H. Navigating the Unnatural Reaction Space: Directed Evolution of Heme Proteins for Selective Carbene and Nitrene Transfer. *Acc. Chem. Res.* **2021**, *54*, 1209−1225.

(3) Chen, K.; Arnold, F. H. Engineering New Catalytic Activities in Enzymes. *Nat. Catal.* **2020**, *3*, 203−213.

(4) Singh, R.; Mukherjee, A. Metalloporphyrin Catalyzed C-H Amination. *ACS Catal.* **2019**, *9*, 3604−3617.

(5) Hyster, T. K.; Farwell, C. C.; Buller, A. R.; McIntosh, J. A.; Arnold, F. H. Enzyme-Controlled Nitrogen-Atom Transfer Enables Regiodivergent C-H Amination. *J. Am. Chem. Soc.* **2014**, *136*, 15505−15508.

(6) Singh, R.; Bordeaux, M.; Fasan, R. P450-Catalyzed Intramolecular Sp3 C−H Amination with Arylsulfonyl Azide Substrates. *ACS Catal.* **2014**, *4*, 546−552.

(7) Steck, V.; Kolev, J. N.; Ren, X.; Fasan, R. Mechanism-Guided Design and Discovery of Efficient Cytochrome P450-Derived C-H Amination Biocatalysts. *J. Am. Chem. Soc.* **2020**, *142*, 10343−10357.

(8) Conradie, J.; Ghosh, A. Electronic Structure of an Iron-Porphyrin−Nitrene Complex. *Inorg. Chem.* **2010**, *49*, 243−248.

(9) Li, X.; Dong, L.; Liu, Y. Theoretical Study of Iron Porphyrin Nitrene: Formation Mechanism, Electronic Nature, and Intermolecular C-H Amination. *Inorg. Chem.* **2020**, *59*, 1622−1632.

(10) Kuijpers, P. F.; van der Vlugt, J. I.; Schneider, S.; de Bruin, B. Nitrene Radical Intermediates in Catalytic Synthesis. *Chem. Eur. J.* **2017**, *23*, 13819−13829.

(11) Mahajan, M.; Mondal, B. Origin of the Distinctive Electronic Structure of Co- and Fe-Porphyrin-Nitrene and Its Effect on Their Nitrene Transfer Reactivity. *Inorg. Chem.* **2023**, *62*, 5810−5821.

(12) Svastits, E. W.; Dawson, J. H.; Breslow, R.; Gellman, S. H. Functionalized Nitrogen Atom Transfer Catalyzed by Cytochrome P-450. *J. Am. Chem. Soc.* **1985**, *107*, 6427−6428.

(13) Singh, R.; Bordeaux, M.; Fasan, R. P450-Catalyzed Intramolecular sp3 C−H Amination with Arylsulfonyl Azide Substrates. *ACS Catal.* **2014**, *4*, 546−552.

(14) Bordeaux, M.; Singh, R.; Fasan, R. Intramolecular C(sp3)−H Amination of Arylsulfonyl Azides with Engineered and Artificial Myoglobin-Based Catalysts. *Bioorg. Med. Chem.* **2014**, *22*, 5697−5704.

(15) McIntosh, J. A.; Coelho, P. S.; Farwell, C. C.; Wang, Z. J.; Lewis, J. C.; Brown, T. R.; Arnold, F. H. Enantioselective Intramolecular C-H Amination Catalyzed by Engineered Cytochrome P450 Enzymes in Vitro and in Vivo. *Angew. Chem., Int. Ed.* **2013**, *52*, 9309−9312.
(16) Cho, I.; Prier, C. K.; Jia, Z. J.; Zhang, R. K.; Görbe, T.; Arnold, F. H. Enantioselective Aminohydroxylation of Styrenyl Olefins Catalyzed by an Engineered Hemoprotein. *Angew. Chem., Int. Ed.* **2019**, *58*, 3138−3142.
(17) Moore, E. J.; Fasan, R. Effect of Proximal Ligand Substitutions on the Carbene and Nitrene Transferase Activity of Myoglobin. *Tetrahedron* **2019**, *75*, 2357−2363.
(18) Kalita, S.; Shaik, S.; Dubey, K. D. MD Simulations and QM/MM Calculations Reveal the Key Mechanistic Elements Which Are Responsible for the Efficient C-H Amination Reaction Performed by a Bioengineered P450 Enzyme. *Chem. Sci.* **2021**, *12*, 14507−14518.
(19) Wei, Y.; Conklin, M.; Zhang, Y. Biocatalytic Intramolecular C−H Aminations via Engineered Heme Proteins: Full Reaction Pathways and "axial" Ligand Effects. *Chem. Eur. J.* **2022**, *28*, No. e202202006.
(20) Yang, Y.; Cho, I.; Qi, X.; Liu, P.; Arnold, F. H. An Enzymatic Platform for the Asymmetric Amination of Primary, Secondary and Tertiary C(sp3)−H Bonds. *Nat. Chem.* **2019**, *11*, 987−993.
(21) Frisch, M. J.; Trucks, G. W.; Schlegel, H. B.; Scuseria, G. E.; Robb, M. A.; Cheeseman, J. R.; Scalmani, G.; Barone, V.; Petersson, G. A.; Nakatsuji, H.; Li, X.; Caricato, M.; Marenich, A. V.; Bloino, J.; Janesko, B. G.; Gomperts, R.; Mennucci, B.; Hratchian, H. P.; Ortiz, J. V.; Izmaylov, A. F.; Sonnenberg, J. L.; Williams-Young, D.; Ding, F.; Lipparini, F.; Egidi, F.; Goings, J.; Peng, B.; Petrone, A.; Henderson, T.; Ranasinghe, D.; Zakrzewski, V. G.; Gao, J.; Rega, N.; Zheng, G.; Liang, W.; Hada, M.; Ehara, M.; Toyota, K.; Fukuda, R.; Hasegawa, J.; Ishida, M.; Nakajima, T.; Honda, Y.; Kitao, O.; Nakai, H.; Vreven, T.; Throssell, K.; Montgomery, J. A., Jr.; Peralta, J. E.; Ogliaro, F.; Bearpark, M. J.; Heyd, J. J.; Brothers, E. N.; Kudin, K. N.; Staroverov, V. N.; Keith, T. A.; Kobayashi, R.; Normand, J.; Raghavachari, K.; Rendell, A. P.; Burant, J. C.; Iyengar, S. S.; Tomasi, J.; Cossi, M.; Millam, J. M.; Klene, M.; Adamo, C.; Cammi, R.; Ochterski, J. W.; Martin, R. L.; Morokuma, K.; Farkas, O.; Foresman, J. B.; Fox, D. J. *Gaussian 16, Revision C.01*; Gaussian, Inc.: Wallingford CT, 2016.
(22) Lee, C.; Yang, W.; Parr, R. G. Development of the Colle-Salvetti Correlation-Energy Formula into a Functional of the Electron Density. *Phys. Rev. B* **1988**, *37*, 785−789.
(23) Becke, A. D. Density-Functional Thermochemistry. III. The Role of Exact Exchange. *J. Chem. Phys.* **1993**, *98*, 5648−5652.
(24) Moreau, Y.; Chen, H.; Derat, E.; Hirao, H.; Bolm, C.; Shaik, S. NR Transfer Reactivity of Azo-Compound I of P450. How Does the Nitrogen Substituent Tune the Reactivity of the Species toward C-H and C = C Activation? *J. Phys. Chem. B* **2007**, *111*, 10288−10299.
(25) Sharon, D. A.; Mallick, D.; Wang, B.; Shaik, S. Computation Sheds Insight into Iron Porphyrin Carbenes' Electronic Structure, Formation, and N-H Insertion Reactivity. *J. Am. Chem. Soc.* **2016**, *138*, 9597−9610.
(26) Schäfer, A.; Horn, H.; Ahlrichs, R. Fully Optimized Contracted Gaussian Basis Sets for Atoms Li to Kr. *J. Chem. Phys.* **1992**, *97*, 2571−2577.
(27) Schäfer, A.; Huber, C.; Ahlrichs, R. Fully Optimized Contracted Gaussian Basis Sets of Triple Zeta Valence Quality for Atoms Li to Kr. *J. Chem. Phys.* **1994**, *100*, 5829−5835.
(28) Grimme, S.; Ehrlich, S.; Goerigk, L. Effect of the Damping Function in Dispersion Corrected Density Functional Theory. *J. Comput. Chem.* **2011**, *32*, 1456−1465.
(29) Marenich, A. V.; Cramer, C. J.; Truhlar, D. G. Universal Solvation Model Based on Solute Electron Density and on a Continuum Model of the Solvent Defined by the Bulk Dielectric Constant and Atomic Surface Tensions. *J. Phys. Chem. B* **2009**, *113*, 6378−6396.
(30) Li, C.; Wu, W.; Cho, K.; Shaik, S. Oxidation of Tertiary Amines by Cytochrome P450—Kinetic Isotope Effect as a Spin-State Reactivity Probe. *Chem. Eur. J.* **2009**, *15*, 8492−8503.
(31) Harvey, J. N.; Aschi, M.; Schwarz, H.; Koch, W. The Singlet and Triplet States of Phenyl Cation. A Hybrid Approach for Locating Minimum Energy Crossing Points between Non-Interacting Potential Energy Surfaces. *Theor. Chem. Acc.* **1998**, *99*, 95−99.
(32) Rodríguez-Guerra, J. *Jaimergp/easymecp: V0.3.2*. Zenodo November 27, 2020.
(33) Roos, B. O. The Complete Active Space Self-Consistent Field Method and Its Applications in Electronic Structure Calculations. *Adv. Chem. Phys.* **1987**, *69*, 399−445.
(34) Kupper, C.; Mondal, B.; Serrano-Plana, J.; Klawitter, I.; Neese, F.; Costas, M.; Ye, S.; Meyer, F. Nonclassical Single-State Reactivity of an Oxo-Iron(IV) Complex Confined to Triplet Pathways. *J. Am. Chem. Soc.* **2017**, *139*, 8939−8949.
(35) Mondal, B.; Neese, F.; Bill, E.; Ye, S. Electronic Structure Contributions of Non-Heme Oxo-Iron(V) Complexes to the Reactivity. *J. Am. Chem. Soc.* **2018**, *140*, 9531−9544.
(36) Angeli, C.; Cimiraglia, R.; Evangelisti, S.; Leininger, T.; Malrieu, J.-P. Introduction of n -Electron Valence States for Multireference Perturbation Theory. *J. Chem. Phys.* **2001**, *114*, 10252−10264.
(37) Neese, F. The ORCA Program System. *WIREs Comput. Mol. Sci.* **2012**, *2*, 73−78.
(38) Wang, J.; Gao, H.; Yang, L.; Gao, Y. Q. Role of Engineered Iron-Haem Enzyme in Reactivity and Stereoselectivity of Intermolecular Benzylic C−H Bond Amination. *ACS Catal.* **2020**, *10*, 5318−5327.
(39) Huang, H.; Zhao, D.-X.; Yang, Z.-Z. Theoretical Study of Enantioenriched Aminohydroxylation of Styrene Catalyzed by an Engineered Hemoprotein. *J. Phys. Org. Chem.* **2022**, *35*, No. e4280.
(40) Das, S. K.; Das, S.; Ghosh, S.; Roy, S.; Pareek, M.; Roy, B.; Sunoj, R. B.; Chattopadhyay, B. An Iron(II)-Based Metalloradical System for Intramolecular Amination of C(sp2)-H and C(sp3)-H Bonds: Synthetic Applications and Mechanistic Studies. *Chem. Sci.* **2022**, *13*, 11817−11828.
(41) Liu, Z.; Qin, Z. Y.; Zhu, L.; Athavale, S. V.; Sengupta, A.; Jia, Z. J.; Garcia-Borràs, M.; Houk, K. N.; Arnold, F. H. An Enzymatic Platform for Primary Amination of 1-Aryl-2-Alkyl Alkynes. *J. Am. Chem. Soc.* **2022**, *144*, 80−85.
(42) Mai, B. K.; Neris, N. M.; Yang, Y.; Liu, P. C-N Bond Forming Radical Rebound Is the Enantioselectivity-Determining Step in P411-Catalyzed Enantioselective C(sp3)-H Amination: A Combined Computational and Experimental Investigation. *J. Am. Chem. Soc.* **2022**, *144*, 11215−11225.
(43) Goswami, M.; Lyaskovskyy, V.; Domingos, S. R.; Buma, W. J.; Woutersen, S.; Troeppner, O.; Ivanović-Burmazović, I.; Lu, H.; Cui, X.; Zhang, X. P.; Reijerse, E. J.; DeBeer, S.; van Schooneveld, M. M.; Pfaff, F. F.; Ray, K.; de Bruin, B. Characterization of Porphyrin-Co(III)-'Nitrene Radical' Species Relevant in Catalytic Nitrene Transfer Reactions. *J. Am. Chem. Soc.* **2015**, *137*, 5468−5479.
(44) van Leest, N. P.; de Bruin, B. Revisiting the Electronic Structure of Cobalt Porphyrin Nitrene and Carbene Radicals with NEVPT2-CASSCF Calculations: Doublet versus Quartet Ground States. *Inorg. Chem.* **2021**, *60*, 8380−8387.
(45) Vardhaman, A. K.; Barman, P.; Kumar, S.; Sastri, C. V.; Kumar, D.; de Visser, S. P. Comparison of the Reactivity of Nonheme Iron(IV)-Oxo versus Iron(IV)-Imido Complexes: Which Is the Better Oxidant? *Angew. Chem., Int. Ed.* **2013**, *52*, 12288−12292.
(46) Mukherjee, G.; Reinhard, F. G. C.; Bagha, U. K.; Sastri, C. V.; de Visser, S. P. Sluggish Reactivity by a Nonheme Iron(IV)-Tosylimido Complex as Compared to Its Oxo Analogue. *Dalt. Trans.* **2020**, *49*, 5921−5931.
(47) Coin, G.; Patra, R.; Rana, S.; Biswas, J. P.; Dubourdeaux, P.; Clémancey, M.; De Visser, S. P.; Maiti, D.; Maldivi, P.; Latour, J. M. Fe-Catalyzed Aziridination Is Governed by the Electron Affinity of the Active Imido-Iron Species. *ACS Catal.* **2020**, *10*, 10010−10020.
(48) Shaik, S.; Chen, H.; Janardanan, D. Exchange-Enhanced Reactivity in Bond Activation by Metal−Oxo Enzymes and Synthetic Reagents. *Nat. Chem.* **2011**, *3*, 19−27.

https://doi.org/10.1021/jacsau.3c00670
JACS Au 2023, 3, 3494−3505

(49) Wong, S. D.; Bell, C. B.; Liu, L. V.; Kwak, Y.; England, J.; Alp, E. E.; Zhao, J.; Que, L.; Solomon, E. I. Nuclear Resonance Vibrational Spectroscopy on the FeIV = O S = 2 Non-Heme Site in TMG 3 Tren: Experimentally Calibrated Insights into Reactivity. *Angew. Chem., Int. Ed.* **2011**, *50*, 3215−3218.
(50) Hirao, H.; Kumar, D.; Que, L.; Shaik, S. Two-State Reactivity in Alkane Hydroxylation by Non-Heme Iron−Oxo Complexes. *J. Am. Chem. Soc.* **2006**, *128*, 8590−8606.
(51) Louwerse, M. J.; Jan Baerends, E. Oxidative Properties of FeO2+: Electronic Structure and Solvation Effects. *Phys. Chem. Chem. Phys.* **2007**, *9*, 156−166.
(52) Hirao, H.; Que, L.; Nam, W.; Shaik, S. A Two-State Reactivity Rationale for Counterintuitive Axial Ligand Effects on the C-H Activation Reactivity of Nonheme FeIV = O Oxidants. *Chem. Eur. J.* **2008**, *14*, 1740−1756.
(53) Janardanan, D.; Wang, Y.; Schyman, P.; Que, L.; Shaik, S. The Fundamental Role of Exchange-Enhanced Reactivity in C-H Activation by S = 2 Oxo Iron(IV) Complexes. *Angew. Chem., Int. Ed.* **2010**, *49*, 3342−3345.

https://doi.org/10.1021/jacsau.3c00670
JACS Au 2023, 3, 3494−3505